analytical chemistry

Article

Cite This: *Anal. Chem.* 2019, 91, 3604−3610

pubs.acs.org/ac

Nucleic Acid-Functionalized Metal−Organic Framework-Based Homogeneous Electrochemical Biosensor for Simultaneous Detection of Multiple Tumor Biomarkers

Jiafu Chang,[†,‡] Xin Wang,[†] Jiao Wang,[†] Haiyin Li,[*,†] and Feng Li[*,†,‡]

[†]College of Chemistry and Pharmaceutical Sciences, Qingdao Agricultural University, Qingdao 266109, People's Republic of China

[‡]College of Chemistry, Chemical Engineering and Materials Science, Shandong Normal University, Jinan 250014, People's Republic of China

Supporting Information

ABSTRACT: Simultaneous detection of multiple tumor biomarkers is in great demand for early and accurate cancer diagnosis. A homogeneous electrochemical biosensor has been proven to possess high sensitivity, but achieving simultaneous detection of multiple tumor biomarkers is still a challenge. Herein, we develop a novel homogeneous electrochemical biosensor for simultaneous detection of multiple tumor biomarkers based on the functionalized metal−organic frameworks (MOFs). The functionalized MOFs were prepared by using porous UIO-66-NH_2 as nanocontainer to load electroactive dyes and dsDNA as a gatekeeper to cap MOFs. In this context, two functionalized MOFs (MB@UIO and TMB@UIO) were fabricated and applied to simultaneous detection of let-7a and miRNA-21, used as the proof-of-concept analytes. The recognition and hybridization of P_X with target miRNAs impel the generation of RNA−DNA complexes, which separated from MOFs and allowed the electroactive dyes to be released. In comparison with the case when target miRNAs are absent, two stronger signals are recorded, and dependent on target miRNA concentrations. Thus, simultaneous detection of let-7a and minRNA-21 is achieved, with detection limits down to 3.6 and 8.2 fM, respectively, comparable or lower than those of reported strategies that concentrated on single miRNA detection. Moreover, the proposed biosensor has also been successfully applied for simultaneous detection of target miRNAs spiked in serum samples. Therefore, the proposed strategy was expected to provide more information for early and accurate cancer diagnosis and was an useful application in disease diagnosis and clinical biomedicine.

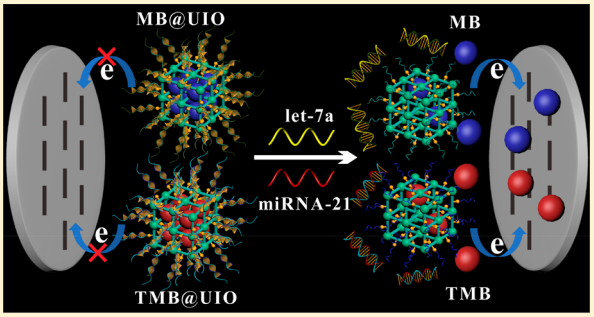

Cancer, known as a life-threatening disease, causes millions of people to die every year due to its high metastatic diffusion capacity and fatality rate, and it significantly affects the human health and public safety.[1] Early and accurate diagnosis of cancer, which may offer valuable information on enhancing the therapeutic efficiency and play a critical role in improving survival rate of cancer patients, is in great demand.[2−4] With the development of biological and medical techniques, tumor biomarkers appeared and served as important indices for risk assessment and early cancer detection.[5,6] Unfortunately, traditional techniques, including X-ray, CT, and B ultrasound concentrating on morphological changes of tissues, cannot meet this demand, and they result in missing the best times for cancer therapy. Given the problems above, considerable efforts have been devoted to developing novel biosensing techniques for cancer early diagnosis through identifying the abnormal expression of tumor biomarkers in biological samples.[7−17] Among these techniques, the homogeneous electrochemical sensing strategy is regarded as an ideal tool due to its immobilization-free characteristic, which not only simplifies the operation procedure and lowers the detection cost but also avoids the steric hindrance effect to strengthen the recognition and response efficiency. However, it is worth noting, that these reported homogeneous electrochemical techniques have several of the following drawbacks. First, most of the previously reported homogeneous electrochemical strategies suffered from the complicated and expensive signal molecule-participated labeling procedure, making the development of homogeneous electrochemical biosensors more difficult. Second, in order to improve the sensitivity, such developed biosensors depend on enzyme-assisted signal amplification strategies, which failed to achieve fast detection and would heighten the cost. Third, all the homogeneous electrochemical biosensors commit themselves to single tumor biomarker detection, easily resulting in false positive diagnosis because the expression level of tumor biomarkers can also be influenced by other factors (inflammation and infection).[18−21] For the sake of addressing the issues above and as a continuation of our studies, we attempt,

Received: December 4, 2018
Accepted: February 13, 2019
Published: February 13, 2019

DOI: 10.1021/acs.analchem.8b05599
Anal. Chem. 2019, 91, 3604−3610

Scheme 1. (I) Schematic Representation of Nucleic Acid-Functionalized MOFs Fabrication Procedure and (II) the Principle of the MOF-Based Homogeneous Electrochemical Biosensor For Multiple Detection of miRNAs

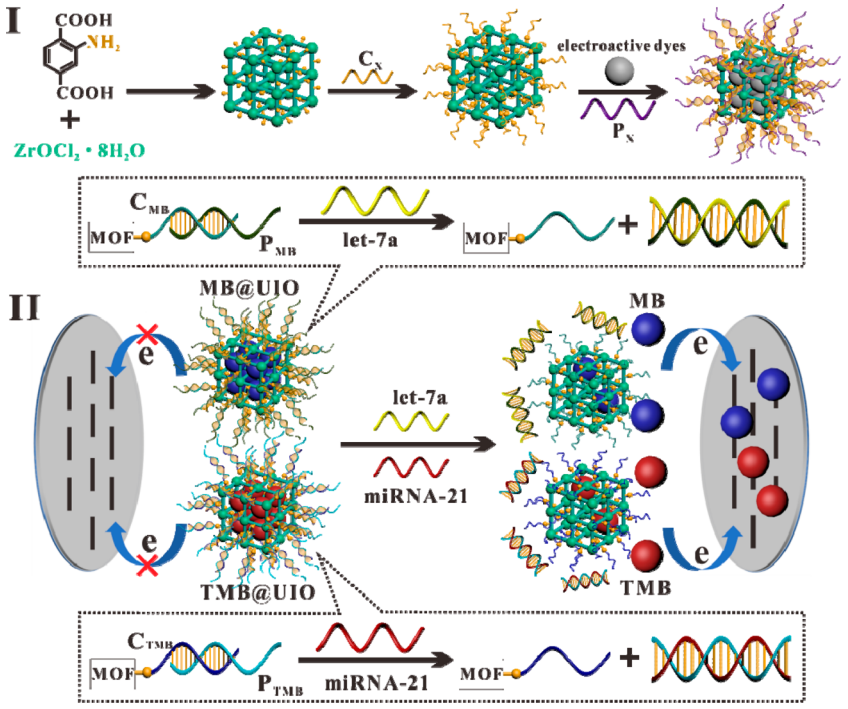

here, to develop a label-free and enzyme-free homogeneous electrochemical strategy for ultrasensitive and simultaneous detection of multiple tumor biomarkers.

Metal−organic frameworks (MOFs) are a broad class of organic/inorganic porous crystalline materials with a large surface area, high porosity, adjustable pore size, and multiple functionalities.[22−25] These unique characteristics make MOFs as ideal material for gas storage,[26] adsorption,[27] separation,[22] catalysis,[28] drug delivery,[29] and chemo/biosensing.[30,31] However, to the best of our knowledge, little information has been done on MOFs in the electrochemical field, especially electrochemical biosensing, because of their weak conductivity.[32] An effective approach to overcome this obstacle is coupling MOFs and conductive substances into a single nanostructure.[33,34] This procedure is complicated and costly and will produce more waste, which seriously hinders the MOFs electrochemical application. Furthermore, it is well established that MOFs could be used as nanocarriers to encapsulate organic molecules and release them through specific stimuli.[35,36] If we introduce MOFs into a homogeneous electrochemical biosensor, such a developed biosensor not only avoids the drawback of weak conductivity but also achieves the label-free and enzyme-free ultrasensitive detection of target analytes. More importantly, regulating different loading molecules and capping substances in MOFs can introduce specific recognition toward different analytes, which provides a possibility to realize the simultaneous detection of multiple tumor biomarkers.

Herein, we proposed a nucleic acid-functionalized MOF-based homogeneous electrochemical strategy with label-free and enzyme-free features for ultrasensitive and simultaneous detection of multiple tumor biomarkers. The functionalized MOF-loading with electroactive dyes and capped with double-stranded DNA (dsDNA-capped MOFs) was constructed via the in situ adsorption and nucleic acid hybridization reaction. The proposed dsDNA-capped MOFs show specific response toward target analytes based on target-initiated electroactive dye release. More interestingly, such proposed MOFs could show different electrochemical signals toward different target analytes through changing the loading dyes and capping DNA structures, benefiting the development of electrochemical biosensors for simultaneous detection of multiple tumor biomarkers. In view of this, two functionalized MOFs (MB@UIO and TMB@UIO) were ingeniously designed and applied for simultaneous detection of let-7a and miRNA-21, used as the proof-of-concept analytes. let-7a and miRNA-21 belong to miRNAs and are promising tumor biomarkers for cancer diagnosis and therapy. Further, a label-free and enzyme-free homogeneous electrochemical strategy was successfully developed for ultrasensitive and simultaneous detection of let-7a and miRNA-21. This study couples the merits of simultaneous biosensing and homogeneous electrochemical strategy to achieve multiple tumor biomarkers detection and, thus, has a great potential for early and accurate cancer diagnosis.

EXPERIMENTAL SECTION

Synthesis of UIO-66-NH_2. First, 1.0 mL of *N*,*N*-dimethylformamide (DMF) solution containing 45 mg of 2-aminoterephthalic acid was mixed with 3.0 mL of DMF solution containing 21 mg of $ZrOCl_2 \cdot 8H_2O$. Subsequently, 750 μL of CH_3COOH was added, and the solution was allowed to react for 15 h at 90 °C to yield UIO-66-NH_2.

Preparation of MB@UIO and TMB@UIO. Prior to fabrication of dsDNA-capped MOFs, EDC and NHS were diluted to 5.0 mg/mL using 20 mM PBS buffer (100 mM NaCl, pH 7.4); C_X (C_{MB} and C_{TMB}) was diluted to 100 μM using this PBS buffer; P_X (P_{MB} and P_{TMB}) was diluted to 1.5 μM using this PBS buffer, too.

DOI: 10.1021/acs.analchem.8b05599
Anal. Chem. 2019, 91, 3604−3610

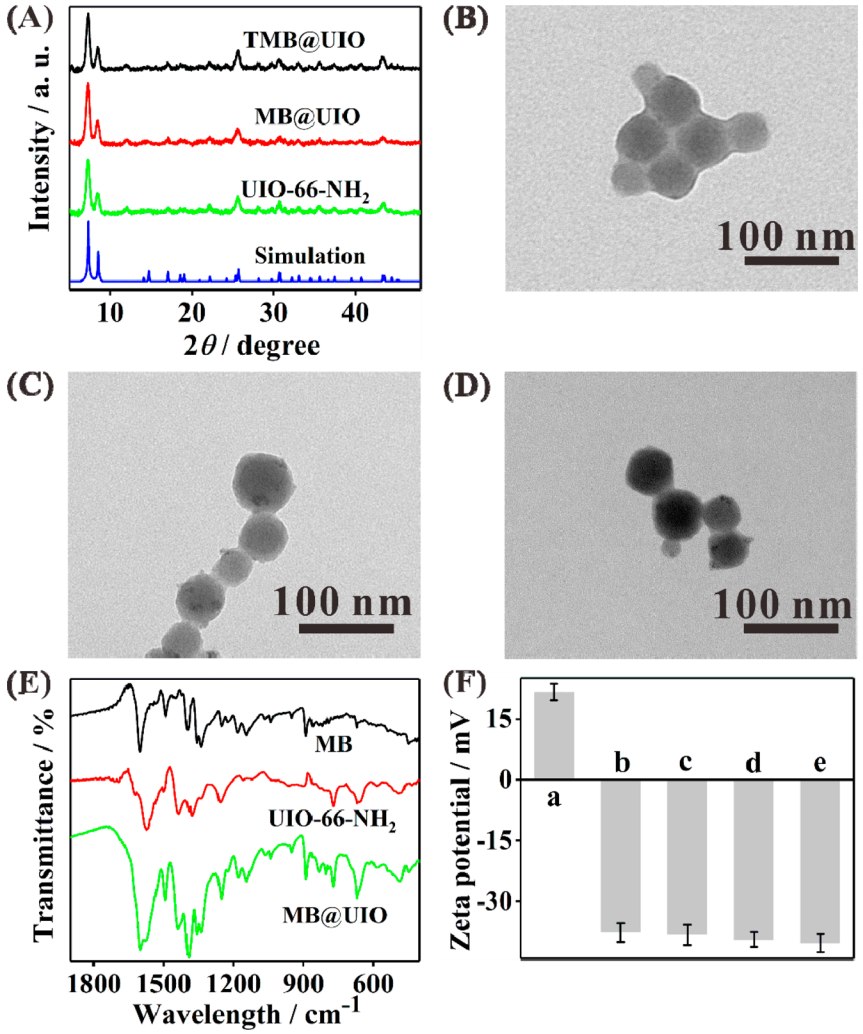

Figure 1. (A) XRD patterns of different samples. TEM images of the UIO-66-NH_2 (B), MB@UIO (C), and TMB@UIO (D). (E) FT-IR spectra of MB, UIO-66-NH_2, and MB@UIO. (F) Zeta potential values of different samples, (a) UIO-66-NH_2, (b) C_{MB}-modified UIO-66-NH_2, (c) C_{TMB}-modified UIO-66-NH_2, (d) MB@UIO, and (e) TMB@UIO.

For MB@UIO preparation, 500 μL of C_{MB}, 250 μL of EDC, and 250 μL of NHS were mixed together and reacted for 20 min. Subsequently, 10 mg of UIO-66-NH_2 was added, and the reaction solution was allowed to react for 15 h. The modified UIO-66-NH_2 was washed with PBS three times through centrifugation and redispersed in 1.0 mL of PBS for further application. To load MB, 100 μL of C_{MB}-modified UIO-66-NH_2 was incubated with 20 μL of MB solution (1.0 mM) for 12 h under continuous stirring. Then, 80 μL of P_{MB} was added, and the mixture was allowed to react for 3.0 h to form dsDNA-capped MOFs (MB@UIO). The prepared MB@UIO was rinsed with PBS three times through centrifugation and dispersed in 1 mL of PBS buffer for the subsequent experiments. According to the process, TMB@UIO was also successfully prepared.

Simultaneous Detection of let-7a and miRNA-21. For electrochemical biosensing, 20 μL of MB@UIO, 20 μL of TMB@UIO, and 40 μL of target miRNAs containing let-7a and miRNA-21 with different concentrations were incubated for 1.0 h. Following that, the solution was diluted with PBS to 200 μL. Finally, the DPV signals of the sensing system were determined with the potential ranging from −0.3 to +0.45 V (vs Ag/AgCl).

For fluorescent biosensing, 20 μL of MB@UIO, 20 μL of TMB@UIO, and 40 μL of target miRNAs containing let-7a and miRNA-21 with different concentrations were incubated for 1.0 h. Following that, the solution was diluted with PBS to 200 μL. The fluorescence spectra were recorded after the centrifugation (8000 rpm, 2 min). For MB, the fluorescence was excited at 610 nm and recorded in the range of 640−820 nm; for TMB, the fluorescence was excited at 290 and recorded in the range of 310−565 nm.

RESULTS AND DISCUSSION

Principle of MOFs-Based Homogeneous Electrochemical Biosensor. The working principle of the MOF-based homogeneous electrochemical biosensor for ultrasensitive and simultaneous detection of multiple tumor biomarkers is depicted in Scheme 1. In our design, UIO-66-NH_2 consisting of Zr^{4+} and 2-aminoterephthalic acid were synthesized and chosen as nanocarriers to encapsulate electroactive dyes. Subsequently, the carboxylated ssDNA C_X was linked onto the surface of UIO-66-NH_2 through the amidation reaction. Then, electroactive dyes were entrapped into the pores of UIO-66-NH_2 through soaking MOFs in a solution of electroactive dyes. After this procedure, another

DOI: 10.1021/acs.analchem.8b05599
Anal. Chem. 2019, 91, 3604−3610

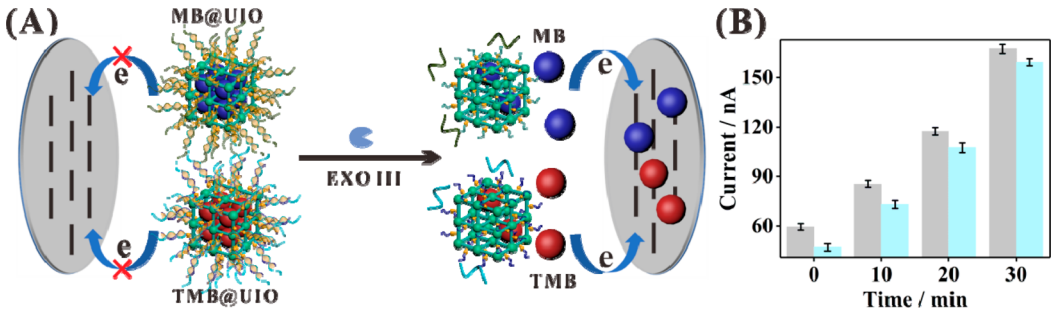

Figure 2. (A) The interaction between Exo III and dsDNA-capped MOFs. (B) The peak currents versus the reaction time between Exo III and dsDNA-capped MOFs.

ssDNA P_X, which was completely complementary to the target biomarker, partially hybridized with C_X and acted as the gatekeeper to form dsDNA-capped MOFs. According to the proposed strategy, two different electroactive dyes (MB and TMB) and four ingeniously designed DNA (C_{MB}, P_{MB}, C_{TMB}, and P_{TMB}) were introduced to produce MB@UIO and TMB@UIO, respectively, both of which could be used as homogeneous electrochemical biosensors for let-7a and miRNA-21 simultaneous detection. In the absence of target analytes, the dsDNA on MOFs prevented the release of MB and TMB. As such, the peak currents of MB and TMB were ultralow. Once one of the target analytes was introduced, it would hybridize with P_X to form the RNA−DNA complex through the toehold-mediated strand-displacement reaction. The formed RNA−DNA complex was far away from MOFs due to its rigid structure, leading to the release of the entrapped dyes. It is worth noting, that only one dye (MB or TMB) could be released, subsequently resulting in one stronger electrochemical signal. Upon the addition of the two biomarkers, both MB and TMB were allowed to simultaneously release into the sensing system. Further, the released MB and TMB would result in both strong peak currents. Consequently, the MOF-based homogeneous electrochemical biosensor for simultaneous detection of the two tumor biomarkers was developed on the account of two signal variations.

Characterization of dsDNA-Capped MOFs. To verify the formation of dsDNA-capped MOFs, an X-ray diffraction (XRD) technique was conducted. As shown in Figure 1A, the synthesized UIO-66-NH_2, MB@UIO, and TMB@UIO displayed sharp diffraction peaks in XRD patterns, which are highly consistent with the simulated data from the single crystal, implying good purity and high crystallinity. No peaks from MB or TMB molecules were determined, suggesting that no MB/TMB crystals existed in MB@UIO/TMB@UIO materials. Further, transmission electron microscopy (TEM) analysis was applied to investigate their morphologies (Figure 1B−D). An identical diameter (55 nm) was observed for UIO-66-NH_2, MB@UIO, and TMB@UIO, respectively. This indicated that MB or TMB made little influence on the morphologies of the prepared MOFs. To gain more insights into dsDNA-capped MOFs, scanning electron microscopy (SEM), energy dispersive spectroscopy (EDS), X-ray photoelectron spectroscopy (XPS), and energy dispersive X-ray spectrometry (EDX) were conducted to verify that the DNA effectively assembled as the gatekeeper (Figures S1−3), and FT-IR spectra were carried out to confirm the electroactive dyes effectively encapsulated (Figure 1E). Evidently, new peaks, including 1599, 1180, 1142, 1034, 950, and 885 cm^{-1}, appeared in MB@UIO compared with that in UIO-66-NH_2, justifying MB was effectively encapsulated in UIO-66-NH_2. The same conclusion can also be obtained from that of TMB@UIO (Figure S4). Meanwhile, a new element P appeared in TMB@UIO compared with that in UIO-66-NH_2 and was assigned to the DNA, suggesting that DNA was linked on the surface of UIO-66-NH_2 through the amide reaction and nucleic acid hybridization to form the biogate. Furthermore, a zeta potential was applied to study the surface functionalization of the prepared MOFs (Figure 1F). UIO-66-NH_2 was electropositive and the value was determined to be +21.67 mV. As expected, the potential became −37.64 mV/−38.24 mV after the linkage of ssDNA, and the hybridizing with P_X would further increase the negative charge.

Prior to the application of dsDNA-capped MOFs in analysis of miRNAs, their stability was evaluated through dispersing them in PBS buffer for different times or in human serum samples. As shown in Figure S5, the MB@UIO and TMB@UIO were stable in the absence of target analytes, and thus, no significant current change was observed. More importantly, their currents had negligible change, too, in human serum samples, even after the time was extended to be 7 h. These results indicated that dsDNA could be used as the gatekeeper to prevent the electroactive dyes release, and the functionalized MOFs enjoyed excellent stability. Exonuclease III (Exo III), capable of catalyzing the stepwise removal of mononucleotides from the 3′-OH termini of dsDNA, was applied to further evaluate the influence of DNA structures on encapsulating efficiency. The interaction between Exo III and dsDNA-capped MOFs is illustrated in Figure 2A. Evidently, only a small amount of ssDNA existed on MOF surfaces after the Exo III-mediated cleavage reaction, subsequently leading to a large amount of electroactive dye released into the solution and two strong electrochemical signals (Figure 2B). The reason for this phenomenon is due to the disappearance of dsDNA-capped MOF surfaces.

Feasibility Study of let-7a and miRNA-21 Simultaneous Detection. To confirm the feasibility of the proposed biosensor for let-7a and miRNA-21 simultaneous detection, the DPV signals of MB (I_{MB}) and TMB (I_{TMB}) with different concentrations were recorded. As shown in Figure 3A, MB and TMB have different potentials located at −0.21 and 0.32 V, respectively. Meanwhile, the DPV signals increased with the increase of their concentrations, justifying the possibility of MB and TMB utilized as electroactive dyes in the development of homogeneous electrochemical biosensors for simultaneous detection of let-7a and miRNA-21. Subsequently, the electrochemical signals of the proposed biosensor in the absence/presence of target analytes were determined (Figure 3B). If no

DOI: 10.1021/acs.analchem.8b05599
Anal. Chem. 2019, 91, 3604−3610

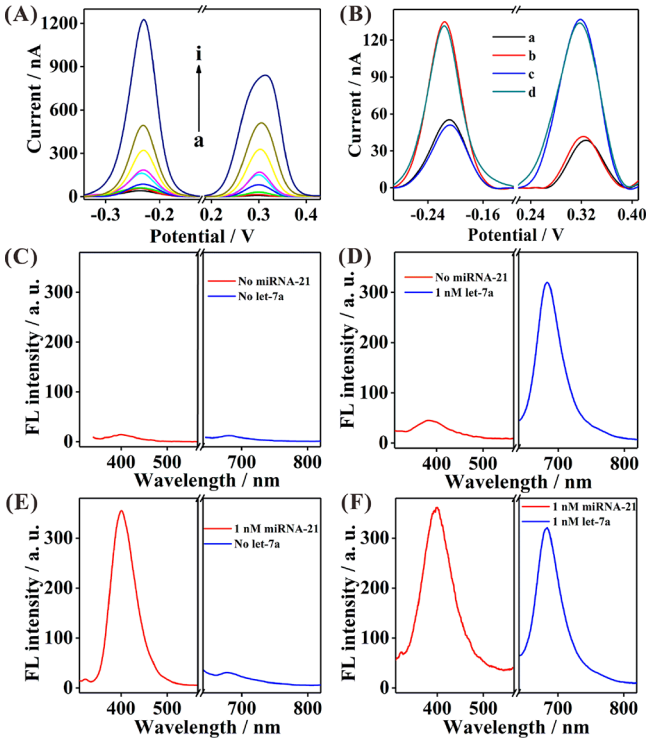

Figure 3. (A) DPV responses of MB and TMB at different concentrations, 50, 100, 200, 500, 800 nM, 1, 2, 3, and 5 μM. (B) DPV responses of MB@UIO and TMB@UIO under different conditions, no target analytes (a); 2 pM let-7a (b); 2 pM miRNA-21 (c); and 2 pM let-7a + 2 pM miRNA-21 (d). (C–F) The fluorescence spectra of MB@UIO and TMB@UIO under different conditions.

target analytes existed in the sensing system, the oxidation currents of MB and TMB were 55.51 and 38.58 nA, respectively. Whereas, only in the presence of let-7a, the oxidation current of MB increased to 134.73 nA, accompanied by that of TMB remaining slightly changed. In contrast, if only miRNA-21 existed, the oxidation current of TMB increased to 137.00 nA, accompanied by that of MB remaining slightly changed. This is because the effective release of electroactive dyes is dependent on the target-initiated hybridization reaction. Thus, when both of let-7a and miRNA-21 existed, the oxidation currents of MB and TMB increased to 132.07 and 134.73 nA, respectively. The above information obviously indicates that the MOF-based homogeneous electrochemical strategy can achieve let-7a and miRNA-21 simultaneous detection.

To further verify the feasibility of the proposed strategy, fluorescence characterizations were carried out, and the results are illustrated in Figure 3C–F. TMB and MB have different emission wavelengths of 398.65 and 683.60 nm, respectively. Compared with the fluorescence intensities of MB@UIO and TMB@UIO, both stronger signals were obtained in the presence of let-7a and miRNA-21, with the intensities located at 320.19 and 360.45 a.u., respectively. The significantly increased FL intensities are indubitably ascribed to the efficient release of MB and TMB from MOFs through the target-induced hybridization reaction. Furthermore, when only one target analyte is present, there is only one stronger fluorescence signal recorded. From this context, it can be inferred that the proposed biosensor met the demand for let-7a and miRNA-21 simultaneous detection through the fluorescence intensity variation. However, it should be noted, that there are some problems for simultaneous fluorescence biosensing. (1) MB, TMB, and other fluorescence dyes used for simultaneous biosensing have different UV–vis spectra and fluorescence spectra, which might result in fluorescence resonance energy transfer and mutual interference, thus reducing the diagnosis accuracy. (2) In general, they have different excitation wavelengths, making the simultaneous biosensing disadvantageous in one single assay. (3) In addition, most of the fluorescence strategies suffered from the complex centrifugation procedure. By contrast, MOF-based homogeneous electrochemical biosensors can successfully avoid these drawbacks for let-7a and miRNA-21 simultaneous detection.

Optimization of Experimental Conditions. Prior to simultaneous detection of let-7a and miRNA-21 using our established platform, the amount of electroactive dyes and P_X and the hybridization time between target analytes and dsDNA-capped MOFs were optimized to get the best performance. First, the amount of electroactive dyes encapsulated in UIO-66-NH_2 made a significant influence on DPV signals, and thus was studied. From Figure S6A, the DPV current increased with MB concentration increasing, implying that more MB were entrapped in UIO-66-NH_2. When MB concentration increased to 100 μM, the DPV signal got the maximum value. Thus, 100 μM served as the optimal MB concentration to improve the sensing sensitivity. Next, the amount of P_{MB} for capping MB in the pores of UIO-66-NH_2 was investigated. As depicted in Figure S6C, with the concentration of P_{MB} increased from 100 to 1000 nM, the DPV currents increased in the initial stage and leveled off when the amount reached 600 nM. Thus, 600 nM served as the optimum concentration. Finally, the hybridization time between let-7a and MB@UIO was also monitored. As shown in Figure S6E, the electrochemical signal was elevated at a high speed initially, and it reached a plateau at 60 min, suggesting 60 min is sufficient for the hybridization reaction between let-7a and MB@UIO. For the TMB-participated biosensor, the amounts of TMB and P_{TMB}, and the hybridization time were optimized to be 100 μM, 600 nM, and 60 min, respectively.

Simultaneous Detection of let-7a and miRNA-21. To confirm the ability of MB@UIO and TMB@UIO to simultaneously detect let-7a and miRNA-21, a series of experiments were conducted under the optimized conditions. Figure 4A gave the electrochemical responses determined upon the addition of let-7a and miRNA-21 with different concentrations. Compared with that of the blank sample (MB@UIO and TMB@UIO), the DPV currents increased obviously with both the let-7a and miRNA-21 concentrations increasing, which could be attributable to the sensing principle that more target analytes triggered the release of more electroactive dyes (MB and TMB), thus enhancing the DPV currents. Standard working curves made by plotting DPV currents versus the let-7a and miRNA-21 concentrations are depicted in Figure 4B,C. The I_{MB} and I_{TMB} were found to be linearly relevant to the logarithm let-7a and miRNA-21 concentrations ($lgC_{let\text{-}7a}$ and $lgC_{miRNA\text{-}21}$) in the range of 0.01–10 and 0.02–10 pM, respectively. For let-7a analysis, the regression equation was determined as $I_{MB} = 32.4017lgC_{let\text{-}7a} + 118.5219$ with a coefficient (R^2) of 0.9824 and a detection limit (LOD) of 3.6 fM based on 3σ; for miRNA-21 analysis, the regression equation was $I_{TMB} = 38.3024lgC_{miRNA\text{-}21}+117.0456$ with an R^2 of 0.9917 and an LOD of 8.2 fM based on 3σ. The LOD, as shown in Table S2,

DOI: 10.1021/acs.analchem.8b05599
Anal. Chem. 2019, 91, 3604–3610

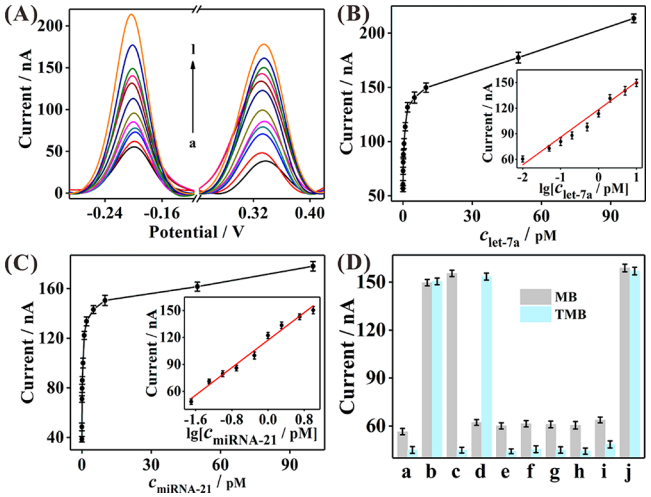

Figure 4. (A) The DPV responses of the proposed biosensor corresponding to let-7a and miRNA-21 with different concentrations, (a) 0 + 0, (b) 0.01 + 0.02, (c) 0.05 + 0.05, (d) 0.1 + 0.1, (e) 0.2 + 0.2, (f) 0.5 + 0.5, (g) 1 + 1, (h) 2 + 2, (i) 5 + 5, (j) 10 + 10, (k) 50 + 50, and (l) 100 + 100 pM. (B) DPV currents versus let-7a concentrations. Inset shows the linear curve of DPV currents versus lgC_{let-7a}. (C) DPV currents versus miRNA-21 concentrations. Inset shows the linear curve of DPV currents versus $lgC_{miRNA-21}$. (D) Comparison of DPV currents in the presence of (a) no target analytes; (b) let-7a and miRNA-21; (c) let-7a, miRNA-16, and miRNA-155; (d) miRNA-21, let-7b, and let-7d; (e) ALT; (f) L-serine; (g) taurine; (h) glucose; (i) let-7b, let-7d, miRNA-16, miRNA-155, ALT, L-serine, taurine, and glucose; and (j) let-7a, miRNA-21, let-7b, let-7d, miRNA-16, miRNA-155, ALT, L-serine, taurine, and glucose. The concentration of ALT was 20 U/L, and the concentrations of other interfering substances were 10 pM.

was comparable or superior to those of the reported methods that concentrated on single miRNA detection and suffered from a complicated and expensive signal molecule-participated labeling procedure, enzyme-assisted signal amplification strategy, and long responsive time. This high sensitivity may be originated from the UIO-66-NH_2's highly porous structure permitting for the encapsulation of a large number of electroactive dyes, and the superior gating effect of dsDNA to ssDNA allowing for an increase in the amount of electroactive dyes released in the presence of only a small amount of target analytes. Overall, this MOF-based electrochemical biosensor manifests evident advantages of simple operation, rapid response, and low cost, and it can become a more powerful tool for the simultaneous and ultrasensitive detection of multiple miRNAs, benefiting accurate and early cancer diagnosis.

Selectivity of MOF-Based Homogeneous Electrochemical Biosensor. To investigate the selectivity of the MOF-based homogeneous electrochemical biosensor for let-7a and miRNA-21 simultaneous detection, we performed a series of experiments using let-7b, let-7d, miRNA-16, miRNA-155, alanine aminotransferase (ALT), L-serine, taurine, and glucose as the interferences. As shown in Figure 4D, both I_{MB} and I_{TMB} exhibited significant change in the presence of let-7a and miRNA-21. When only let-7a existed, the sensing system showed an obvious I_{MB} increase compared with I_{TMB}; in contrast, when only miRNA-21 existed, the sensing system showed an obvious I_{TMB} increase compared with I_{MB}. Nevertheless, in the absence of target analytes, both I_{MB} and I_{TMB} demonstrated slight changes compared with that of MB@UIO and TMB@UIO. Moreover, the mixture made little influence on the sensing performance of the proposed biosensor toward let-7a and miRNA-21. Thus, the proposed biosensor exhibited excellent performance for distinguishing let-7a and miRNA-21 against other miRNAs interferences. Further, the reusability of C_x-modified UIO-66-NH_2 was studied through the heat/separation treatment of MB@UIO and TMB@UIO in the presence of target analytes (Figure S7). The results demonstrated that it can be reused three times with a slight variation in DPV current.

Real Sample Analysis. In view of the high sensitivity and good selectivity, the MOF-based homogeneous electrochemical biosensor was expected to simultaneously detect let-7a and miRNA-21 in biological samples. To verify this, we determine the recoveries and relative standard deviations (RSDs) of let-7a and miRNA-21 with different concentrations spiked into 30% diluted human serum samples. As depicted in Table S3, for let-7a and miRNA-21 with different concentrations, the measured recoveries were calculated to be 94.7, 103, and 105% and 96.3, 97.4, and 104%, respectively, with the RSDs in the range of 3.20−4.75%. Further, the proposed MOF-based biosensor was employed to simultaneously detect let-7a and miRNA-21 in serum from a breast cancer patient through the standard addition method (Figure S8). When the concentrations of let-7a and miRNA-21 are higher than 10 pM, the serum was diluted with PBS buffer before analyzing. The levels of let-7a and miRNA-21 in breast cancer patient serum were determined to be 19.68 and 23.24 nM, respectively. These evaluations suggested a significant potential of the MOF-based homogeneous electrochemical biosensor for simultaneous detection of multiple miRNAs in biological samples for accurate and early cancer diagnosis.

■ CONCLUSIONS

In this work, a novel homogeneous electrochemical biosensor has been designed for ultrasensitive and simultaneous detection of multiple miRNAs in one single assay based on dsDNA-capped MOFs. With UIO-66-NH_2 and dsDNA taken as the nanocontainer and gatekeeper, MB@UIO and TMB@UIO were successfully prepared and served as homogeneous electrochemical biosensors to simultaneously detect let-7a and miRNA-21, in which MB and TMB were effectively encapsulated in the pores of UIO-66-NH_2. Owing to UIO-66-NH_2's highly porous structure and the superior gating effect of dsDNA to ssDNA, the proposed biosensor demonstrated excellent sensing performance with high sensitivity and good selectivity. The LODs were 3.6 fM for let-7a and 8.2 fM for miRNA-21, which was comparable or superior to those of the reported methods that concentrated on single miRNA detection. Furthermore, the MOF-based biosensor was applied in simultaneous analysis of let-7a and miRNA-21 in human serum samples with high accuracy and reliability. Moreover, simultaneous and ultrasensitive detection of other tumor biomarkers can be readily achieved by simply changing the loading dyes and capping DNA structures, thus supplying an universal homogeneous electrochemical platform for the simultaneous and ultrasensitive detection of various biomarkers. Therefore, the proposed biosensor has great potential for accurate and early cancer diagnosis.

DOI: 10.1021/acs.analchem.8b05599
Anal. Chem. 2019, 91, 3604−3610

■ ASSOCIATED CONTENT

Supporting Information

The Supporting Information is available free of charge on the ACS Publications website at DOI: 10.1021/acs.analchem.8b05599.

Sequences of the oligonucleotides; multiple miRNAs assay performance of the present strategy with other methods; SEM, EDS, EDX, XPS, and FT-IR characterizations; and optimization of experimental conditions (PDF)

■ AUTHOR INFORMATION

Corresponding Authors

*E-mail: lihaiyin@qau.edu.cn.

*Tel/Fax: 86-532-86080855; E-mail: lifeng@qau.edu.cn.

ORCID

Feng Li: 0000-0002-3894-6139

Notes

The authors declare no competing financial interest.

■ ACKNOWLEDGMENTS

This work was funded by the National Natural Science Foundation of China (21605093, 21575074, and 21775082), the Special Foundation for Distinguished Taishan Scholar of Shandong Province (ts201511052), and the Major Program of Shandong Province Natural Science Foundation (ZR2018ZC0127).

■ REFERENCES

(1) Jemal, A.; Bray, F.; Center, M. M.; Ferlay, J.; Ward, E.; Forman, D. *Ca-Cancer J. Clin.* **2011**, *61*, 69−90.

(2) Jo, H.; Gu, H.; Jeon, W.; Youn, H.; Her, J.; Kim, S.-K.; Lee, J.; Shin, J. H.; Ban, C. *Anal. Chem.* **2015**, *87*, 9869−9875.

(3) Liu, Q. Y.; Yang, Y. T.; Li, H.; Zhu, R. R.; Shao, Q.; Yang, S. G.; Xu, J. J. *Biosens. Bioelectron.* **2015**, *64*, 147−153.

(4) Duan, R. X.; Zuo, X. L.; Wang, S. T.; Quan, X. Y.; Chen, D. L.; Chen, Z. F.; Jiang, L.; Fan, C. H.; Xia, F. *J. Am. Chem. Soc.* **2013**, *135*, 4604−4607.

(5) Nathanson, K. N.; Wooster, R.; Weber, B. L. *Nat. Med.* **2001**, *7*, 552−556.

(6) Hofland, J.; Zandee, W. T.; de Herder, W. W. *Nat. Rev. Endocrinol.* **2018**, *14*, 656−669.

(7) Li, H. Y.; Chang, J. F.; Hou, T.; Li, F. *Anal. Chem.* **2017**, *89*, 673−680.

(8) Liu, H. Y.; Li, L.; Wang, Q.; Duan, L. L.; Tang, B. *Anal. Chem.* **2014**, *86*, 5487−5493.

(9) Li, H. Y.; Chang, J. F.; Gai, P. P.; Li, F. *ACS Appl. Mater. Interfaces* **2018**, *10*, 4561−4568.

(10) Causa, F.; Aliberti, A.; Cusano, A. M.; Battista, E.; Netti, P. A. *J. Am. Chem. Soc.* **2015**, *137*, 1758−1761.

(11) Jou, A. F.-j.; Lu, C.-H.; Ou, Y.-C.; Wang, S.-S.; Hsu, S.-L.; Willner, I.; Ho, J.-a. A. *Chem. Sci.* **2015**, *6*, 659−665.

(12) Koo, K. M.; Carrascosa, L. G.; Shiddiky, M. J. A.; Trau, M. *Anal. Chem.* **2016**, *88*, 2000−2005.

(13) Chen, A. Y.; Gui, G. F.; Zhuo, Y.; Chai, Y. Q.; Xiang, Y.; Yuan, R. *Anal. Chem.* **2015**, *87*, 6328−6334.

(14) Miao, X. M.; Cheng, Z. Y.; Ma, H. Y.; Li, Z. B.; Xue, N.; Wang, P. *Anal. Chem.* **2018**, *90*, 1098−1103.

(15) Li, W.; Liu, X. J.; Hou, T.; Li, H. Y.; Li, F. *Biosens. Bioelectron.* **2015**, *70*, 304−309.

(16) Hou, T.; Li, W.; Liu, X. J.; Li, F. *Anal. Chem.* **2015**, *87*, 11368−11374.

(17) Zhu, Q.; Chai, Y. Q.; Zhuo, Y.; Yuan, R. *Biosens. Bioelectron.* **2015**, *68*, 42−48.

(18) Song, Z. J.; Yuan, R.; Chai, Y. Q.; Zhuo, Y.; Jiang, W.; Su, H. L.; Che, X.; Li, J. J. *Chem. Commun.* **2010**, *46*, 6750−6752.

(19) Qiao, G. M.; Gao, Y.; Li, N.; Yu, Z. Z.; Zhuo, L. H.; Tang, B. *Chem. - Eur. J.* **2011**, *17*, 11210−11215.

(20) Pan, W.; Liu, B.; Gao, X. N.; Yu, Z. Z.; Liu, X. H.; Li, N.; Tang, B. *Nanoscale* **2018**, *10*, 14264−14271.

(21) Chang, N.; Gu, Z.-Y.; Yan, X.-P. *J. Am. Chem. Soc.* **2010**, *132*, 13645−13647.

(22) Morris, W.; Briley, W. E.; Auyeung, E.; Cabezas, M. D.; Mirkin, C. A. *J. Am. Chem. Soc.* **2014**, *136*, 7261−7264.

(23) Wang, S.; McGuirk, C. M.; Ross, M. B.; Wang, S.; Chen, P.; Xing, H.; Liu, Y.; Mirkin, C. A. *J. Am. Chem. Soc.* **2017**, *139*, 9827−9830.

(24) Yang, S. J.; Kim, T.; Im, J. H.; Kim, Y. S.; Lee, K.; Jung, H.; Park, C. R. *Chem. Mater.* **2012**, *24*, 464−470.

(25) Tian, T.; Zeng, Z.; Vulpe, D.; Casco, M. E.; Divitini, G.; Midgley, P. A.; Silvestre-Albero, J.; Tan, J.-C.; Moghadam, P. Z.; Fairen-Jimenez, D. *Nat. Mater.* **2017**, *17*, 174−179.

(26) Zhao, M. T.; Yuan, K.; Wang, Y.; Li, G. D.; Guo, J.; Gu, L.; Hu, W. P.; Zhao, H. J.; Tang, Z. Y. *Nature* **2016**, *539*, 76−80.

(27) Liu, D.; Huxford, R. C.; Lin, W. B. *Angew. Chem., Int. Ed.* **2011**, *50*, 3696−3700.

(28) Horcajada, P.; Chalati, T.; Serre, C.; Gillet, B.; Sebrie, C.; Baati, T.; Eubank, J. F.; Heurtaux, D.; Clayette, P.; Kreuz, C.; Chang, J.-S.; Hwang, Y. K.; Marsaud, V.; Bories, P.-N.; Cynober, L.; Gil, S.; Férey, G.; Couvreur, P.; Gref, R. *Nat. Mater.* **2010**, *9*, 172−178.

(29) Wu, S.; Li, C.; Shi, H.; Huang, Y.; Li, G. X. *Anal. Chem.* **2018**, *90*, 9929−9935.

(30) Wu, S.; Lin, Y.; Liu, J.; Shi, W.; Yang, G.; Cheng, P. *Adv. Funct. Mater.* **2018**, *28*, 1707169.

(31) Zhang, S.-Y.; Shi, W.; Cheng, P.; Zaworotko, M. J. *J. Am. Chem. Soc.* **2015**, *137*, 12203−12206.

(32) Fernandes, D. M.; Barbosa, A. D. S.; Pires, J.; Balula, S. S.; Cunha-Silva, L.; Freire, C. *ACS Appl. Mater. Interfaces* **2013**, *5*, 13382−13390.

(33) Wang, Y.; Wang, L.; Huang, W.; Zhang, T.; Hu, X. Y.; Perman, J. A.; Ma, S. Q. *J. Mater. Chem. A* **2017**, *5*, 8385−8393.

(34) Jahan, M.; Bao, Q.; Loh, K. P. *J. Am. Chem. Soc.* **2012**, *134*, 6707−6713.

(35) Chen, W.-H.; Yu, X.; Cecconello, A.; Sohn, Y. S.; Nechushtai, R.; Willner, I. *Chem. Sci.* **2017**, *8*, 5769−5780.

(36) Kahn, J. S.; Freage, L.; Enkin, N.; Garcia, M. A. A.; Willner, I. *Adv. Mater.* **2017**, *29*, 1602782.

DOI: 10.1021/acs.analchem.8b05599
Anal. Chem. 2019, 91, 3604−3610